Published in final edited form as:
J Am Chem Soc. 2010 December 22; 132(50): 17724–17732. doi:10.1021/ja102138a.

Oil Phase Evaporation Induced Self-Assembly of Hydrophobic Nanoparticles into Spherical Clusters with Controlled Surface Chemistry in an Oil-in-Water Dispersion and Comparison of Behaviors of Individual and Clustered Iron Oxide Nanoparticles

Penghe Qiu[†], **Christina Jensen**[†], **Njoku Charity**[‡], **Rheal Towner**[‡], and **Chuanbin Mao**[*,†]
Department of Chemistry and Biochemistry, University of Oklahoma, Stephenson Life Sciences Research Center, 101 Stephenson Parkway, Norman, OK, 73019, and Advanced Magnetic Resonance Center, Oklahoma Medical Research Foundation, Oklahoma City, OK 73104

Abstract

We report a general method for preparing nanoparticle clusters (NPCs) in an oil-in-water emulsion system mediated by cetyl trimethylammonium bromide (CTAB) where previously, only individual nanoparticles were obtained. NPCs of magnetic, metallic and semiconductor nanoparticles have been prepared to demonstrate the generality of the method. The NPCs were spherical and composed of densely packed individual nanoparticles. The number density of nanoparticles in the oil phase was found to be critical for the formation, morphology and yield of NPCs. The method developed here is scalable and can produce NPCs in nearly 100% yield at a concentration of 5 mg/ml in water which is approximately 5 times higher than the highest value reported in literature. The surface chemistry of NPCs can also be controlled by replacing CTAB with polymers containing different functional groups via a similar procedure. The reproducible production of NPCs with well defined shapes has allowed us to compare the properties of individual and clustered iron oxide nanoparticles including magnetization, magnetic moments and contrast enhancement in magnetic resonance imaging (MRI). We found that due to their collective properties, NPCs are more responsive to an external magnetic field and can potentially serve as better contrast enhancement agents than individually dispersed magnetic NPs in MRI.

Introduction

The self-assembly of nanoparticles into hierarchical 2-D or 3-D structures has been extensively studied for potential applications in various fields.[1–5] The self-assembly behavior can take place both at the interfaces and *in situ*. Assembly at the interfaces of liquid-air and liquid-liquid often results in mono- or multi-layered nanostructures.[6–9] *In situ* aggregation results in the formation of nanoparticle clusters (NPCs) which are larger particles containing a finite number of nanoparticles.[10–12] In literature, the *in situ* assembly of nanoparticles has been almost exclusively induced by introducing specifically designed stimulating molecules into the nanoparticles suspension. For example, by adding dodecanethiol into oleylamine capped gold nanoparticles in cholorform, clusters of gold nanoparticles can be assembled due to their reduced stability after ligand exchange.[10]

cbmao@ou.edu.
[†]Department of Chemistry and Biochemistry, University of Oklahoma.
[‡]Advanced Magnetic Resonance Center, Oklahoma Medical Research Foundation

Supporting Information Available: Larger view of iron oxide NPCs made from CTAB emulsion; silica coated NPCs; size selection of CdS NPCs; Au NPCs; NPCs prepared by using PAA, PEI and PSS as stabilizers; iron oxide nanoparticles individually dispersed in water after phase transfer. This information is available free of charge via the Internet at http://pubs.acs.org/.

However, a particular type of stimulus may only be good for specific nanoparticles having certain surface ligands. Here we report a simple and general method of assembling hydrophobic nanoparticles into water-dispersed spherical NPCs. In this method, the formation of NPCs is achieved without adding any stimulating reagents by selective evaporation of the organic phase in an oil-in-water micelle system. The surface chemistry of NPCs can be readily tuned by using different polymers. The method used here can also be extended to make NPCs containing multiple types of nanoparticles.

CTAB is a well-known surfactant and has been widely used in nanoscience. CTAB can aid in the synthesis of many types of nanoparticles with controlled morphologies.[13–17] One important application in nanoscience is its use as a phase transfer reagent. Many types of nanoparticles have been transferred from the organic to aqueous phase with the assistance of CTAB.[1,18–22] However, in all of these works, only individually dispersed nanoparticles could be obtained after the phase transfer process and no cluster structure has so far been reported under similar CTAB concentration. In this work, we found that if the concentration of nanoparticles is increased to a certain level within CTAB micelles, the NPCs can be formed via evaporation of the organic phase during the phase transfer process.

NPCs exhibit collective properties which individual nanoparticles do not have. Clusters of metallic nanoparticles that are rich in surface plasmon such as gold and silver can create Raman hotspots in between the closely spaced particles due to local electromagnetic coupling.[23,24] Such an effect results in an enhancement of Raman signals from analytes in orders of magnitude.[24–27] Unlike single superparamagnetic iron oxide nanoparticles which exhibit low magnetization and are thus difficult to manipulate with a magnet, NPCs have a much higher response to magnetic fields and are therefore better suited for drug delivery and separation.[28] In addition, clusters of superparamagnetic iron oxide nanoparticles have shown improved contrast enhancement compared to individual nanoparticles in magnetic resonance imaging (MRI).[11,29–32] Various methods have been employed for synthesizing iron oxide NPCs for MRI applications. Generally, these methods fall into two categories. One type involves block copolymers, either bihydrophilic or amphiphilic.[30,33,34] The other category utilizes simultaneous cluster formation with a silica coating process.[11,31,32] In most of these reported works, a relatively low concentration of iron oxide nanoparticles was used for cluster formation which may prevent them from scalable production. The micelle system we have selected in this current work can result in a final NPCs concentration of 5 mg/ml in an aqueous phase, which is approximately 5 times higher than the highest reported concentrations from previous works.[29,31,32] In addition, the density of iron oxide nanoparticles inside the cluster is much higher than reported values.

Experimental Methods

Synthesis of oil dispersed Fe_3O_4, CdS and Au nanoparticles

Fe_3O_4 nanoparticles were synthesized and purified following the procedure done by Sun et al.[35] Nanoparticles of 3 nm and 6 nm in diameter could be obtained directly by controlling the solvent and reaction temperature. Larger Fe_3O_4 nanoparticles (12 nm and 15 nm in diameter) were produced by seeded growth based on the 6 nm nanoparticles. Nanoparticles derived from 2 mmol iron acetylacetonate were redispersed into hexane at a concentration of 20 mg/ml where the concentration of the nanoparticles used for NPC formation could be diluted or re-concentrated from the stock solution.

CdS nanoparticles were synthesized following the reported method in literature with slight modifications.[36] A mixture of cadmium chloride (91.66 mg, 0.5 mM) and oleylamine (5 ml) was heated to 150 °C under N_2 flow. When $CdCl_2$ was completely dissolved (in about 20 min), 0.5 mM elemental sulfur dissolved in 2.5 ml of oleylamine was quickly added into the

hot solution. The reaction was maintained at 150 °C for an additional 8 hours. Next, it was quenched by quickly adding 15 ml of toluene. Nanoparticles were purified by washing three times with ethanol. Finally, they were suspended into 2 ml of hexane and used for NPCs formation.

Au nanoparticles were synthesized by mixing 100 μl 0.1 M $HAuCl_4$ with 5 ml oleylamine and heated at 150 °C for about 25 min. The nanoparticles were then washed twice with ethanol and finally dispersed into 0.2 ml hexane.

Synthesis of NPCs using CTAB as an emulsifier

A small volume of hexane-dispersed nanoparticles (200 μl, concentration varies from 1–100 mg/ml) was added to 4 ml of 0.1 M CTAB aqueous solution. All of the liquid was then gently mixed by hand shaking followed by sonication for 2 min to form a stable micelle suspension. Afterwards, the mixture was heated in a 80 °C water bath and stirred at 500 rpm for 5 min to have the majority of the hexane evaporated. Alternatively, hexane evaporation can be done by stirring under the ambient condition for several hours. The solution was then removed from the heat and stirred under a vacuum for 30 min to completely remove the hexane. In the preparation of Au-CdS hybrid NPCs, 50 μl AuNPs was mixed with 150 μl CdS nanoparticles and sonicated before being added to the CTAB solution.

Synthesis of NPCs using polymers as stabilizers

A volume of 200 μl of hexane-dispersed iron oxide nanoparticles (2 mg/ml) was added to 4 ml of 12 wt% polymer solution. The mixture was then sonicated continuously for 2 h. The water bath of the sonicator was initially set at 40 °C, however, the temperature was increased to around 70 °C after 1 h due to the heating effect of ultrasound. After sonication, the solution was also treated by vacuum for 30 min. The molecular weights of the polymers used are as follows: polyacrylic acid (PAA, 15 k, sodium salt, 35 wt%), polyethyleneimine (PEI, 25 k, branched) and poly(styrenesulfonate) (PSS, 70 k).

Silica coating of CTAB stabilized Fe_3O_4 NPCs

The process of coating NPCs with silica was modified from the method described in literature.[37] Generally, the as-prepared CTAB covered NPCs (1 ml) were centrifuged at 15,000 rpm for 20 min, and redispersed into 4 ml of 0.02 M CTAB aqueous solution. The pH of the solution was adjusted to around 11 by 0.1 M NaOH. Finally, tetraethyl orthosilicate (TEOS, 20 μl) was added and the resultant solution was stirred for 24 h for complete hydrolysis and condensation of TEOS.

Preparation of aqueous individually dispersed NPs

The hexane-dispersed 6 nm iron oxide NPs were resuspended into toluene at a concentration of 10 mg/ml. In a three-neck flask, 500 mg of polyvinylpyrrolidone (PVP, 10 K) was dissolved into 8 ml of DMSO, followed by adding 2 ml of toluene-dispersed NPs. A homogeneous clear solution could then be obtained. This solution was then heated, under N_2 flow, to 189 °C at a temperature increase rate of about 4 °C/min. The temperature was remained at 189 °C for another 30 min, and then cooled to room temperature. The resulting transparent solution was then dialyzed against water (cutoff of the dialysis membrane, 5 kDa) for 24 h, after which aqueous individually dispersed, PVP-stabilized iron oxide NPs could be obtained. Silica-coated individual NPs were prepared by NH_4OH catalyzed hydrolysis of TEOS in an ethanol/water mixed solvent (4:1 v/v).

Characterization

The size and morphology of as-prepared NPCs were characterized by Transmission Electron Microscope (TEM). All the TEM images were obtained on JEOL 2000FX microscope, operated at an accelerating voltage of 200 kV. The surface morphology of NPCs was examined on a Nano-R2 Atomic Force Microscope (AFM) by Pacific Nanotechnology. The magnetic properties of individual and clustered NPs were measured on a Quantum Designs MPMS2 cryogenic susceptometer. The T2-weighted MR images were obtained on a Bruker Biospec 7.0 T, 30 cm horizontal-bore imaging spectrometer.

Results and Discussion

Synthesis of NPCs in CTAB Emulsion

The experimental design is shown in Scheme 1. The idea of making NPCs was inspired by the concept of emulsion in which two immiscible liquids can coexist as a stable dispersion under the assistance of an emulsifier or surfactant in the form of micelles, either oil-in-water (used in this work) or water-in-oil. Oil will appear as tiny droplet suspended in bulk water. In oil-in-water emulsion, the surfactant molecules (CTAB in this work) will line up at the oil/water interface to reduce the surface tension of the tiny oil droplets which would otherwise assemble themselves into large drops.[38] If there are NPs initially dispersed in the bulk oil phase, they will remain inside the oil droplet after emulsification due to their hydrophobic nature. Due to its low boiling point, the oil phase can be removed by evaporation, leading to the condensation of NPs inside the micelles. When oil is completely evaporated, NPs inside each micelle will form a larger cluster. However, the NPs within the cluster will not be fused because the long carbon chains on the NPs surface give rise to a steric barrier that effectively leaves each particle isolated.[6] The surface of the resultant clusters is fully covered by surfactant molecules, with the charged head groups in direct contact with water and the tails interacting with the long carbon chains of NPs in the outer layer (this statement will be validated by the water compatibility and surface charge of NPCs in the next paragraph), similar to the interaction involved when using surfactant to transfer hydrophobic nanoparticles into individual dispersions in water.[22] In this manner, the NPCs are prevented from aggregation and precipitation in the same way as stabilization of individual NPs in aqueous solution.

NPCs made from Fe_3O_4 NPs with an initial individual particle size of 3 nm, 6 nm and 12 nm respectively are shown in Fig. 1 (also see Fig. S1 for larger view). The morphology of NPCs was studied by the atomic force microscope (AFM). As it can be seen from the TEM images in Fig.1, the individual NPs could be differentiated clearly inside the clusters and no fusion is observed in any of the three different sized NPs. The line profile obtained from AFM contains the height information which has been widely used to study the surface morphology of materials. We collected line profiles across two isolated clusters as well as four contacting clusters in a row. In both cases, smooth curves typically for spherical particles were observed (Fig. 1 right). The NPCs obtained in the CTAB-mediated emulsion could be suspended very stably in water, and no aggregation between NPCs was observed once they were centrifuged and resuspended into water. Considering the hydrophobic nature of NPCs, their high water compatibility should originate from the surface protection of the CTAB molecules, which is the only hydrophilic species in the solution. Moreover, the NPCs have a zeta potential of +49 mV, which provides further evidence that the NPCs are stabilized by CTAB, the only positively charged species in the solution. It should be pointed out that although previous micelles created by diblock copolymers were used to make NPCs, the structure reported here is much more closely packed and thus, has a much higher nanoparticle density.

The number density of NPs in the organic phase which is defined as the number of nanoparticles in a unit volume of solution is very important for the formation of NPCs as well as the morphology of clusters. For iron oxide NPs with 6 nm diameter, the NPCs could hardly be seen at a concentration of 1 mg/ml. When the concentration was increased to 4 mg/ml, about 80% of NPs, which was estimated from the darkness of the supernatant after centrifuge, were in the form of clusters. Morphologically, however, the clusters contained both spheres and large film-like multilayered structures (Fig. 2a). At the concentration of 20 mg/ml, more than 98% of NPs existed as spherical clusters after the phase transfer process (Fig. 2b). In contrast, for 20 mg/ml of 15 nm NPs, where the number density was calculated to be 16 times less than that of 6 nm NPs under the same mass concentration, only a small portion were seen to be clusters (Fig. 2c). Therefore, in order to form NPCs during the phase transfer, the number density of NPs in the oil phase has to reach a certain high level which is dependent on the size of the NPs. However, in previously reported works where CTAB was used as the phase transfer reagent, relatively low concentrations of hydrophobic NPs were used. This provides an explanation as to why no clusters of NPs were obtained previously even though the experiments were carried out through a similar method as used in this work.

Size Selection, Scalable Production and Silica Coating of NPCs

The resultant spherical NPCs obtained through selective phase evaporation were widely distributed from several nm up to 150 nm in diameter. However, the size distribution of NPCs can be narrowed by using differential centrifugation in a pure water medium. Clusters assembled from 3 nm Fe_3O_4 NPs were given here as a demonstration. In the first centrifugation run at 10,000 rpm for 5 min, NPCs larger than 50 nm could generally be separated (Figs. 3a&3b) and the average diameter of this fraction was 78 nm. Smaller clusters could then be spun down from the supernatant of the first centrifugation run at 15,000 rpm for 20 min, resulting in a fraction of NPCs with an average diameter of 33 nm (Figs. 3c&3d). A very small portion of even smaller NPCs remained in the supernatant and could not be spun down. The size of nanoparticles has been one of the greater concerns for *in vivo* applications. The exclusion and capture of nanoparticles by organs have a great impact on their circulation in the blood. Nanoparticles smaller than 10 nm will be filtered by the kidney. In addition, they will be captured by the liver, if they are larger than 100 nm. Thus, the optimum nanoparticle size required is 10–100 nm for *in vivo* applications.[39–41] The NPCs should be suitable for *in vivo* applications after the size selection procedures. We believe that the size distribution of NPCs could be further narrowed down by using a density gradient centrifugation.[42,43]

Mass production of hierarchical nanostructures of interest has always been a challenge in nanoparticles assembly. Most often, the assembly suffers from either low yields or poor reproducibility. In this work, the potential for a scalable production of NPCs via the CTAB-based emulsion method was investigated. We kept the volume ratio of hexane to water at a constant value of 0.2 ml over 4 ml but changed the concentration of nanoparticles in the oil phase. Several different concentrations (between 20 to 100 mg/ml) of 3 nm iron oxide NPs were tried. In all of these trials, NPCs were produced in a nearly 100% yield indicated by the supernatants being almost colorless after centrifugation at 15000 rpm. A TEM study showed that all of the clusters were composed of closely-packed nanoparticles where no coagulation was observed. Also, there was not a significant increase of cluster size even at a higher initial concentration. When the total volume was expanded by 10 times (100 mg/ml iron oxide NPs in 2 ml hexane and 40 ml water), we generally did not observe any remarkable difference in the NPC size distribution and morphology compared to clusters formed in the 4 ml water system. It should be noted that in current literature, relatively low concentrations of iron oxide NPs were used to synthesize NPCs. Mostly, the initial concentration of NPs in the organic phase was below 10 mg/ml while the final concentration of NPCs in the aqueous

phase was less than 1 mg/ml.[32] The initial and final concentrations can reach up to 100 and 5 mg/ml respectively in the current work, which makes it more promising for the scalable production of NPCs.

The as-prepared NPCs were very stable for further surface modification. Polyelectrolyte wrapping through electrostatic interactions has been one method for manipulating the surface charge of nanoparticles.[44,45] The CTAB capped NPCs can be wrapped with multiple layers of polyelectrolytes without destroying their cluster structure. Moreover, silica can be coated uniformly around the NPCs in a basic solution (Fig. S2). The NPCs/silica core/shell structure enables greater functionality on the particles by the well-developed silica modification chemistry.[46,47] For example, fluorescent dyes have been linked onto silica through covalent bonding between amine groups from 3-aminopropyltriethoxysilane (APTES) and isothiocyanate or succinimidyl-ester groups on the dyes; the dye-silica-magnetic NP complex particles can be used as dual probes for both fluorescent imaging and MRI. [48,49]

Generality of the Method

The method we developed here can readily be applied to produce NPCs of varying materials from their hydrophobic nanoparticles. As representatives of semiconductive and metallic materials, CdS and gold NPCs are prepared in CTAB micelles through the same procedures as making NPCs of magnetic particles. In order to explore the potential of preparing multiple-component particles by our method, hydrophobic CdS and Au NPs were first mixed together in hexane followed by selective phase evaporation in CTAB micelles. In all three types of NPCs, a spherical morphology and dense packing of NPs, similar to those of Fe_3O_4 NPCs, were observed (Fig. 4). The fluorescent property of CdS nanoparticles was retained after the formation of clusters. The size distribution of CdS NPCs could also be narrowed by the differential centrifugation (Fig. S3). The absorption spectrum of gold NPCs was red shifted compared to that of the individually dispersed AuNPs (Fig. S4). For CdS and many other semiconductor nanocrystals, the size-dependent fluorescence due to a quantum confinement effect can only be observed when the size of the particles is smaller than the Bohr radius[50] (e.g., below 10 nm for commonly used CdSe nanocrystals). However, *in vivo* imaging and diagnostics prefers NPs of larger sizes (10–100 nm).[39,41] For instance, blood vessels in tumor tissue are leakier and have larger pores than those in normal tissue. A larger particle can be selectively delivered to tumor tissue for therapeutic or diagnosis purposes due to enhanced permeability and retention (EPR) effect.[41] Therefore, it is difficult to obtain semiconductor NPs having both fluorescence and a desired size for *in vivo* applications simultaneously. NPC structure provides a means for increasing the particle size, while still retaining the fluorescence capability that only belongs to smaller nanoparticles. Forming NPCs from NPs could potentially be a better solution than surface modifications of NPs, which only slightly increases the particle size, as a means for solving the size-fluorescence paradox of semiconductor nanocrystals. The red shift in the absorption spectrum of Au NPCs is contributed by the surface plasmon coupling of adjacent NPs inside the clusters. Such a coupling effect can be used for enhancing the signal intensity of analytes in surface enhanced Raman scattering (SERS) detection. The composite clusters that contain more than one type of nanoparticles have more functionalities, and thus can be used for multiple purposes. For example, Fe_3O_4 and CdSe nanoparticles were successfully embedded into a silica particle, which makes it possess both magnetic and fluorescent properties that could be potentially employed in MRI and fluorescent imaging.[51,52]

Control of Surface Chemistry of NPCs

In practice, especially for biological applications, NPs often require further modifications with functional molecules. For example, in targeted delivery, the drug molecules will be

immobilized onto the NPs surface.[53] Typically, two strategies can be employed for the immobilization of desired molecules onto NPs: electrostatic interactions between two oppositely charged species and chemical bonding (covalent conjugation with surface functional groups, like $–NH_2$ and –COOH).[53] Both methods require sophisticated control over the surface chemistry of NPs. For this reason, it is always interesting to prepare NPs with controllable surface charge and functional groups. Here, we demonstrate our ability to manipulate the surface chemistry of NPCs by employing functional polymers, including PEI, PAA, and PSS, instead of CTAB as surface capping reagents. Morphologically, the polymer stabilized NPCs were similar to those obtained from CTAB emulsion (Figs. S5–S7, for clusters made from 6 nm NPs). The PEI stabilized NPCs showed positive charges; while NPCs covered by PAA and PSS exhibited negative charges as indicated by the zeta potential measurement. In addition, amine (from PEI) or carboxylic acid (from PAA) groups were also present on the surface of the NPCs. The size of polymer stabilized NPCs could also be regulated by differential centrifugation (Table 1). In the CTAB micelles, small NPCs (below 100 nm) can be prepared even at an initial NPs concentration of 100 mg/ml. In the polymers solution, however, small NPCs could only be produced when the initial NPs concentration was much lower (2 mg/ml as used in the experiment). At a higher NPs concentration (20 mg/ml), most of NPCs were greater than 500 nm in diameter, which makes them unsuitable for biological applications. These polymers are not emulsifiers, so no stable oil-in-water dispersion can be formed. Therefore, it was necessary to place the mixture solution under sonication throughout the entire experiment in order to prevent the coagulation of oil droplets. However, in terms of stabilization of NPCs, the polymers behave similar to the CTAB. Their hydrophobic backbone can interact with long carbon chains on the NPCs and their hydrophilic side groups can provide compatibility with the aqueous phase.[54,55] The controllable surface chemistry of NPCs makes them capable of linking molecules through both electrostatic interaction and covalent bonding.

Comparison of Behaviors of Individual and Clustered Iron Oxide NPs

In order to make comparisons between NPs in both individual and clustered forms, hydrophobic iron oxide NPs (i.e., those used for preparing clusters), were transferred into water as individually dispersed particles (Fig. 5a, also see Fig. S8 for silica coated individual iron oxide NPs as a more direct evidence). Their magnetic response to an external field was measured at 5 K and 300 K sweeping between −10 kOe and 10 kOe. Both types of particles showed superparamagnetic behavior at 300 K without coercivity. At 5 K, a typical ferromagnetic-like hysteresis loop was observed (Fig. 6a). The NPCs and individual NPs had very close coercivity (31 vs. 27 Oe). In the zero-field-cooled/ field-cooled (ZFC/FC) magnetization measurements, the blocking temperature significantly increased from 111 K (corresponding to individual NPs) to 181 K after the cluster formation (Fig. 6b). It is well accepted that for assembled nanoparticulate structures, magnetic dipole–dipole interactions are much stronger than those of individual nanoparticles as a result of the distance dependent nature of such interactions.[56] The anisotropy coupling of dipoles, such as nanoparticles densely packed in 1-D pores, results in a ferromagnetic effect which strongly enhances the coercivity.[57] However, non-oriented dipole-dipole interactions, as in most random nanoparticle aggregates, has been demonstrated both experimentally and theoretically to result in decreased coercivity because of the antiferromagnetic coupling effect.[57,58] In our work, neither a significant increase nor decrease of coercivity of NPCs as compared to individual NPs was observed. This is likely due to the presence of both anisotropic and random dipole-dipole interactions within the clusters, which makes NPCs behave like a non-interacting system. During the formation of NPCs, the kinetically fast condensation due to the quick evaporation of hexane inside the micelles as well as the high thermal energy originating from the high experimental temperature could inevitably cause random assembly. On the other hand, since the liquid was homogenized under magnetic

stirring through the entire process, the NPs were magnetized, which could have introduced some anisotropy to the assembly through the partial alignment of magnetic moments of NPs.[59–61] Thus, the sum of the negative contributions from the random assembly and positive contributions from anisotropic assembly within the NPCs may result in a magnetization curve similar to that of noninteracting individually dispersed NPs. The blocking temperature shifting effect in the ZFC/FC measurement is consistent with the results reported in the literature, which show that inter-particle magnetic coupling can suppress the thermal fluctuation of magnetic spins and raise the ferromagnetic to superparamagnetic transition to a higher temperature.[57,62–64]

The single cluster has a much higher magnetic moment than individual iron oxide NPs, which was theoretically predicated earlier by Ge et al.[28] In this work, since we are able to transfer the hydrophobic Fe_3O_4 NPs into stable aqueous dispersions in both clustered and individual forms, direct comparison of the magnetization difference between both forms (and hence their response to an external field) could be made more straightforward. Both Fe_3O_4 NPCs and individually dispersed NPs solutions were placed beside a magnet and observations were periodically made. For individually dispersed iron oxide NPs, we did not observe any visible movement of NPs towards the magnet in 12 h (Fig. 5b). However, all the NPCs could be collected by the magnet within just a few minutes (Fig. 5c). In order to be able to manipulate the movement of particles in solution by a magnet, the magnetic energy on the particle should be larger than the thermal energy, which is the cause of Brownian motion.[56] This behavior for individually dispersed Fe_3O_4 NPs in an external magnetic field is consistent with theoretical result that the magnetic moment of single NPs is so weak that it could not even overcome the random Brownian motion in solution. Since a cluster is made of many individual NPs, the magnetic moment is a collective result of the individuals; therefore, the magnetic force on a cluster is increased many times than that on non-clustered NPs.[28] Consequently, there will be a net positive magnetic force driving the clusters toward the magnet.[56] From this comparison, NPCs could be better suited for applications like drug delivery and molecular separation compared to individual NPs. In these applications, target molecules are often linked onto the particle surface and transported or collected by the movement of magnetic particles in the external field.[61,65–69]

Superparamagnetic iron oxide NPs are well known for being able to shorten the transverse relaxation time of water protons and have been used as a negative contrast agent in MRI.[69] Recently, aggregated or assembled iron oxide NPCs are drawing greater attention in MRI applications because they can provide even higher contrast than individually dispersed magnetic NPs.[29–33,49] In order to test the contrast enhancement effect from the clustering of NPs, we measured the T_2-weighted MR images with different iron concentrations in aqueous dispersion. Both individual and clustered particles exhibited a sensitive concentration-dependent darkness in MR images, where the higher the concentration, the darker the image was. However, under the same iron concentration, darker contrast was observed with NPCs (Fig. 7). Moreover, the clustered nanoparticles showed a transverse relaxivity (r_2) value of 277.6 s^{-1} mM^{-1} Fe, which is remarkably higher than that of individual NPs (15.4 s^{-1} mM^{-1} Fe). This suggests that NPCs could likely be used as a better contrast enhancer in T_2-weighted MR imaging than individual magnetic NPs.

In summary, a general method for making NPCs was developed in a CTAB-mediated oil-in-water emulsion system, where previously only individual NPs were obtained, by increasing the concentration of NPs dispersed in the organic phase. Although NPCs have a wide range of diameters, differential centrifugation can be used to narrow their size distribution. The final concentration of NPCs produced by our method is about 5 times higher than the highest value reported in literature. Moreover, NPCs can be obtained in nearly 100% yield. Therefore, our method for producing NPCs is scalable. The surface chemistry of NPCs can

be manipulated by employing different polymers rather than CTAB, to stabilize them under constant sonication. Iron oxide NPCs have a much higher magnetic moment than individual NPs, making them better suited for separation and drug delivery purposes. In MRI, a significant increase in transverse relaxivity from NPCs also indicates that a lower concentration of iron can be used to give a reasonable contrast.

Supplementary Material

Refer to Web version on PubMed Central for supplementary material.

Acknowledgments

We thank Professor Andrew S. Madden at the School of Geology and Geophysics, University of Oklahoma for his generosity in letting us use the AFM and for the helpful discussion in data processing. We thank the financial support from the National Science Foundation (DMR-0847758, CBET-0854414, CBET-0854465), National Institutes of Health (R21EB009909-01A1, R03AR056848-01, R01HL092526-01A2), and Oklahoma Center for the Advancement of Science and Technology (HR06-161S). RT acknowledges the financial support from National Institutes of Health (5R21CA136642-02).

References

1. Fan HY, Yang K, Boye DM, Sigmon T, Malloy KJ, Xu HF, Lopez GP, Brinker CJ. Science. 2004; 304:567–571. [PubMed: 15105495]
2. Velev OD, Gupta S. Adv Mater. 2009; 21:1897–1905.
3. Le F, Brandl DW, Urzhumov YA, Wang H, Kundu J, Halas NJ, Aizpurua J, Nordlander P. ACS Nano. 2008; 2:707–718. [PubMed: 19206602]
4. Lu Y, Yin YD, Li ZY, Xia YA. Nano Lett. 2002; 2:785–788.
5. Puntes VF, Gorostiza P, Aruguete DM, Bastus NG, Alivisatos AP. Nat Mater. 2004; 3:263–268. [PubMed: 15048109]
6. Bigioni TP, Lin XM, Nguyen TT, Corwin EI, Witten TA, Jaeger HM. Nat Mater. 2006; 5:265–270. [PubMed: 16547519]
7. Duan HW, Wang DY, Kurth DG, Mohwald H. Angew Chem, Int Ed. 2004; 43:5639–5642.
8. Lin Y, Skaff H, Emrick T, Dinsmore AD, Russell TP. Science. 2003; 299:226–229. [PubMed: 12522244]
9. Russell JT, Lin Y, Boker A, Su L, Carl P, Zettl H, He JB, Sill K, Tangirala R, Emrick T, Littrell K, Thiyagarajan P, Cookson D, Fery A, Wang Q, Russell TP. Angew Chem, Int Ed. 2005; 44:2420–2426.
10. Compton OC, Osterloh FE. J Am Chem Soc. 2007; 129:7793–7798. [PubMed: 17550247]
11. Berret JF, Schonbeck N, Gazeau F, El Kharrat D, Sandre O, Vacher A, Airiau M. J Am Chem Soc. 2006; 128:1755–1761. [PubMed: 16448152]
12. Boal AK, Ilhan F, DeRouchey JE, Thurn-Albrecht T, Russell TP, Rotello VM. Nature. 2000; 404:746–748. [PubMed: 10783884]
13. Sau TK, Murphy CJ. J Am Chem Soc. 2004; 126:8648–8649. [PubMed: 15250706]
14. Nehl CL, Liao HW, Hafner JH. Nano Lett. 2006; 6:683–688. [PubMed: 16608264]
15. Murphy CJ, Gole AM, Hunyadi SE, Orendorff CJ. Inorg Chem. 2006; 45:7544–7554. [PubMed: 16961339]
16. Murphy CJ, San TK, Gole AM, Orendorff CJ, Gao JX, Gou L, Hunyadi SE, Li T. J Phys Chem B. 2005; 109:13857–13870. [PubMed: 16852739]
17. Cushing BL, Kolesnichenko VL, O'Connor CJ. Chemical Reviews. 2004; 104:3893–3946. [PubMed: 15352782]
18. Swami A, Kumar A, Sastry M. Langmuir. 2003; 19:1168–1172.
19. Pazos-Perez N, Gao Y, Hilgendorff M, Irsen S, Perez-Juste J, Spasova M, Farle M, Liz-Marzan LM, Giersig M. Chem Mater. 2007; 19:4415–4422.

20. Yan Q, Purkayastha A, Singh AP, Li H, Li A, Ramanujan RV, Ramanath G. Nanotechnology. 2009; 20
21. Fan HY, Wright A, Gabaldon J, Rodriguez A, Brinker CJ, Jiang YB. Adv Funct Mater. 2006; 16:891–895.
22. Kim J, Kim HS, Lee N, Kim T, Kim H, Yu T, Song IC, Moon WK, Hyeon T. Angew Chem, Int Ed. 2008; 47:8438–8441.
23. Moskovits M. J Raman Spectrosc. 2005; 36:485–496.
24. Li WY, Camargo PHC, Au L, Zhang Q, Rycenga M, Xia YN. Angew Chem, Int Ed. 2010; 49:164–168.
25. Yan B, Thubagere A, Premasiri WR, Ziegler LD, Dal Negro L, Reinhard BM. ACS Nano. 2009; 3:1190–1202. [PubMed: 19354266]
26. Alexander KD, Hampton MJ, Zhang SP, Dhawan A, Xu HX, Lopez R. J Raman Spectrosc. 2009; 40:2171–2175.
27. Chen G, Wang Y, Yang MX, Xu J, Goh SJ, Pan M, Chen HY. J Am Chem Soc. 2010; 132:3644. [PubMed: 20196540]
28. Ge JP, Hu YX, Biasini M, Beyermann WP, Yin YD. Angew Chem, Int Ed. 2007; 46:4342–4345.
29. Ai H, Flask C, Weinberg B, Shuai X, Pagel MD, Farrell D, Duerk J, Gao JM. Adv Mater. 2005; 17:1949.
30. Kim J, Lee JE, Lee SH, Yu JH, Lee JH, Park TG, Hyeon T. Adv Mater. 2008; 20:478.
31. Niu DC, Li YS, Ma Z, Diao H, Gu JL, Chen HR, Zhao WR, Ruan ML, Zhang YL, Shi JL. Adv Funct Mater. 2010; 20:773–780.
32. Happy T, Jun Min X, Borys S, Xu L, John W. Adv Funct Mater. 2010; 20:722–731.
33. Ditsch A, Laibinis PE, Wang DIC, Hatton TA. Langmuir. 2005; 21:6006–6018. [PubMed: 15952854]
34. Euliss LE, Grancharov SG, O'Brien S, Deming TJ, Stucky GD, Murray CB, Held GA. Nano Lett. 2003; 3:1489–1493.
35. Sun SH, Zeng H, Robinson DB, Raoux S, Rice PM, Wang SX, Li GX. J Am Chem Soc. 2004; 126:273–279. [PubMed: 14709092]
36. Joo J, Na HB, Yu T, Yu JH, Kim YW, Wu FX, Zhang JZ, Hyeon T. J Am Chem Soc. 2003; 125:11100–11105. [PubMed: 12952492]
37. Gorelikov I, Matsuura N. Nano Lett. 2008; 8:369–373. [PubMed: 18072800]
38. Rosen, MJ. SURFACTANTS AND INTERFACIALPHENOMENA. wiley; 2004.
39. Alexis F, Pridgen E, Molnar LK, Farokhzad OC. Mol Pharm. 2008; 5:505–515. [PubMed: 18672949]
40. Caliceti P, Veronese FM. Adv Drug Delivery Rev. 2003; 55:1261–1277.
41. Gullotti E, Yeo Y. Mol Pharm. 2009; 6:1041–1051. [PubMed: 19366234]
42. Chen G, Wang Y, Tan LH, Yang MX, Tan LS, Chen Y, Chen HY. J Am Chem Soc. 2009; 131:4218. [PubMed: 19275162]
43. Sun XM, Tabakman SM, Seo WS, Zhang L, Zhang GY, Sherlock S, Bai L, Dai HJ. Angew Chem, Int Ed. 2009; 48:939–942.
44. Pastoriza-Santos I, Perez-Juste J, Liz-Marzan LM. Chem Mater. 2006; 18:2465–2467.
45. Gole A, Murphy CJ. Chem Mater. 2005; 17:1325–1330.
46. Santra, S.; Yang, H.; Dutta, D.; Stanley, JT.; Holloway, PH.; Tan, WH.; Moudgil, BM.; Mericle, RA. Chemical Communications. 2004. p. 2810-2811.
47. Hulchanskyy TY, Roy I, Goswami LN, Chen Y, Bergey EJ, Pandey RK, Oseroff AR, Prasad PN. Nano Lett. 2007; 7:2835–2842. [PubMed: 17718587]
48. Lu CW, Hung Y, Hsiao JK, Yao M, Chung TH, Lin YS, Wu SH, Hsu SC, Liu HM, Mou CY, Yang CS, Huang DM, Chen YC. Nano Lett. 2007; 7:149–154. [PubMed: 17212455]
49. Lee JE, Lee N, Kim H, Kim J, Choi SH, Kim JH, Kim T, Song IC, Park SP, Moon WK, Hyeon T. J Am Chem Soc. 2010; 132:552–557. [PubMed: 20017538]
50. Alivisatos AP. Science. 1996; 271:933–937.
51. Selvan ST, Patra PK, Ang CY, Ying JY. Angew Chem, Int Ed. 2007; 46:2448–2452.

52. Yi DK, Selvan ST, Lee SS, Papaefthymiou GC, Kundaliya D, Ying JY. J Am Chem Soc. 2005; 127:4990–4991. [PubMed: 15810812]
53. Ghosh P, Han G, De M, Kim CK, Rotello VM. Adv Drug Delivery Rev. 2008; 60:1307–1315.
54. Guven O, Yigit F. Colloid Polym Sci. 1984; 262:892–895.
55. Qiu PH, Mao CB. ACS Nano. 2010; 4:1573–1579. [PubMed: 20158250]
56. Buschow, KHJ. Handbook of magnetic materials. Elsevier Science; 2006. p. 16
57. Gross AF, Diehl MR, Beverly KC, Richman EK, Tolbert SH. J Phys Chem B. 2003; 107:5475–5482.
58. Lu JJ, Huang HL. Chinese Journal of Physics. 2000; 38:81–94.
59. Corr SA, Byrne SJ, Tekoriute R, Meledandri CJ, Brougham DF, Lynch M, Kerskens C, O'Dwyer L, Gun'ko YK. J Am Chem Soc. 2008; 130:4214. [PubMed: 18331033]
60. Sahoo Y, Cheon M, Wang S, Luo H, Furlani EP, Prasad PN. J Phys Chem B. 2004; 108:3380–3383.
61. Lu Y, Zhao Y, Yu L, Dong L, Shi C, Hu MJ, Xu YJ, Wen LP, Yu SH. Adv Mater. 2010; 22:1407. [PubMed: 20437492]
62. Singh H, Laibinis PE, Hatton TA. Langmuir. 2005; 21:11500–11509. [PubMed: 16285833]
63. Xia HB, Yi JB, Foo PS, Liu BH. Chem Mater. 2007; 19:4087–4091.
64. Srivastava S, Samanta B, Arumugam P, Han G, Rotello VM. J Mater Chem. 2007; 17:52–55.
65. Son SJ, Reichel J, He B, Schuchman M, Lee SB. J Am Chem Soc. 2005; 127:7316–7317. [PubMed: 15898772]
66. Dobson J. Drug Dev Res. 2006; 67:55–60.
67. Arruebo M, Fernandez-Pacheco R, Ibarra MR, Santamaria J. Nano Today. 2007; 2:22–32.
68. McBain SC, Yiu HHP, Dobson J. International Journal of Nanomedicine. 2008; 3:169–180. [PubMed: 18686777]
69. Sun C, Lee JSH, Zhang MQ. Adv Drug Delivery Rev. 2008; 60:1252–1265.

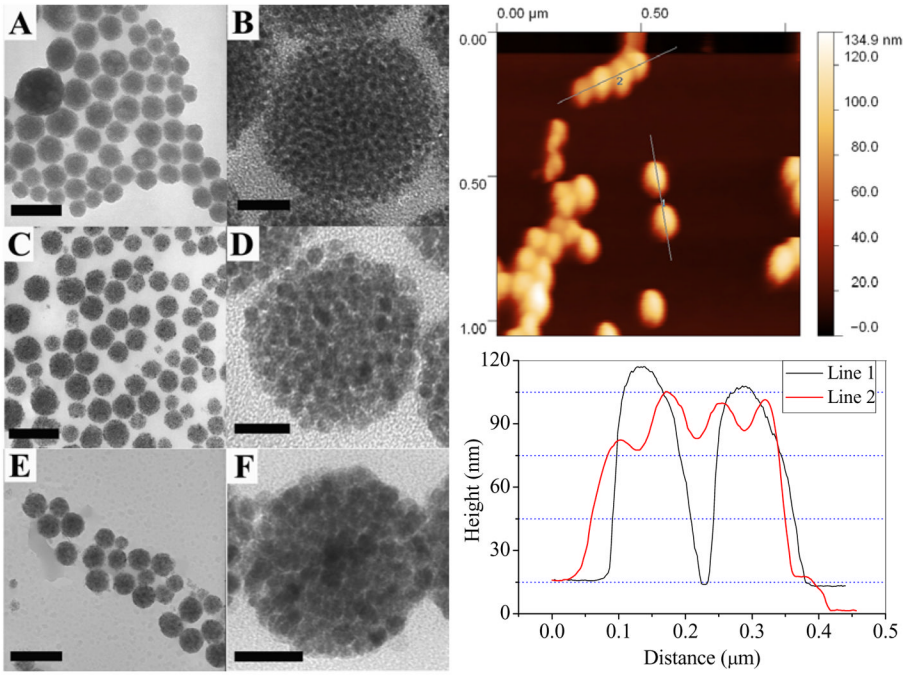

Figure 1.

Left: (A–F) TEM images of low and high magnification of iron oxide NPCs using CTAB as an emulsifier. The initial size of nanoparticles in the organic phase were: (A, B) 3 nm, (C, D) 6 nm, and (E, F) 12 nm respectively. Scale bars: A, C, 150 nm; B, D 20 nm; E, 300 nm; F, 40 nm. Also See Figure S1 for larger view. **Right**: top: AFM image of NPCs made from 6 nm iron oxide NPs; bottom: extracted height information from two isolated clusters (line 1) and four contacting clusters in a row (line 2). The TEM images along with AFM characterization indicate that the NPCs were spheres composed of densely packed individual nanoparticles.

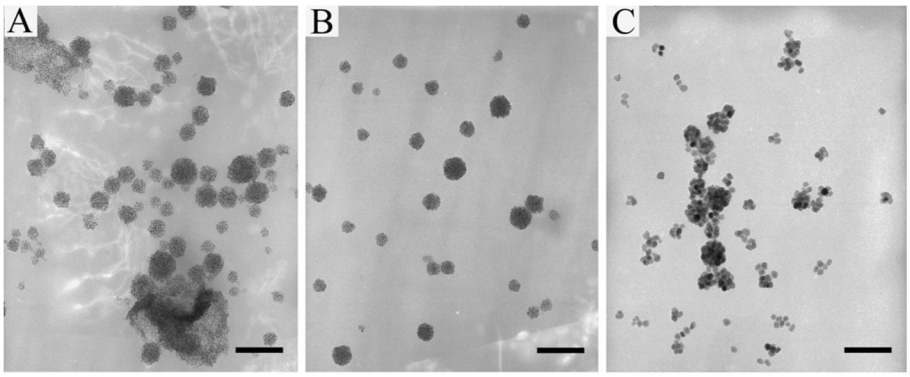

Figure 2.

Dependence of NPCs yield and morphology on the number density of NPs dispersed in the oil phase. (A) NPCs made from 6 nm NPs at 4 mg/ml, more than 80% were clusters, however, non-spherical assembly was also observed; (B) NPCs made from 6 nm iron oxide NPs at 20 mg/ml, all spherical with more than 98% yield; (C) NPCs made from 15 nm NPs at 20 mg/ml, which is calculated to have about 16 times lower number density than that of 6 nm NPs. NPCs were produced at a very low yield with many individual NPs. Scale bars: 100 nm.

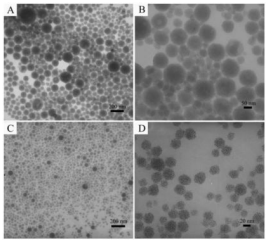

Figure 3.

Size selection of Fe_3O_4 NPCs by differential centrifuge. (A, B), low and high magnification TEM images of NPCs made from 3 nm NPs, showing that NPCs larger than 50 nm can be collected in the first centrifuge run at 10,000 rpm for 5 min; (C, D), low and high magnification TEM images of NPCs showing that smaller ones will be spun down in the second round centrifuge at 15,000 rpm for 20 min.

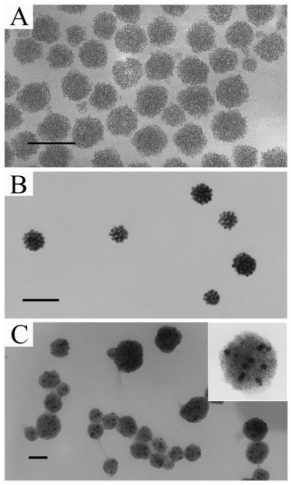

Figure 4.

Generality of the micelle-phase evaporation method in making NPCs of various materials. (A), NPCs of 3 nm CdS, also see Fig. S3 for size selection and fluorescent image; (B), NPCs of 10 nm Au, also see Fig. S4 for optical shift and larger view; (C), Hybrid NPCs of 10 nm Au (dark spots) and 3 nm CdS (self-assembled to form the gray area). Scale bars: 100 nm.

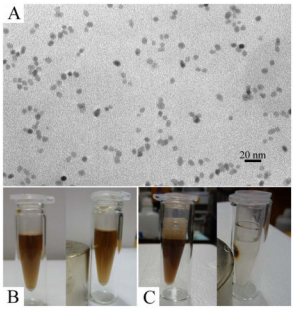

Figure 5.

Comparison between NPCs and individually dispersed iron oxide NPs of their response to an external magnetic field. (A) TEM images of individually dispersed 6 nm iron oxide NPs, identical to those used to form clusters after being transferred from oil to water; (B) Photos show that no visible movement of individual NPs was observed in 12 h, indicating a very weak magnetic moment of individual NPs; (C) Photos show that all the NPCs were attracted to the magnet in just a few minutes, indicating a strong magnetic moment resulting from the collective effect of nanoparticles in NPCs.

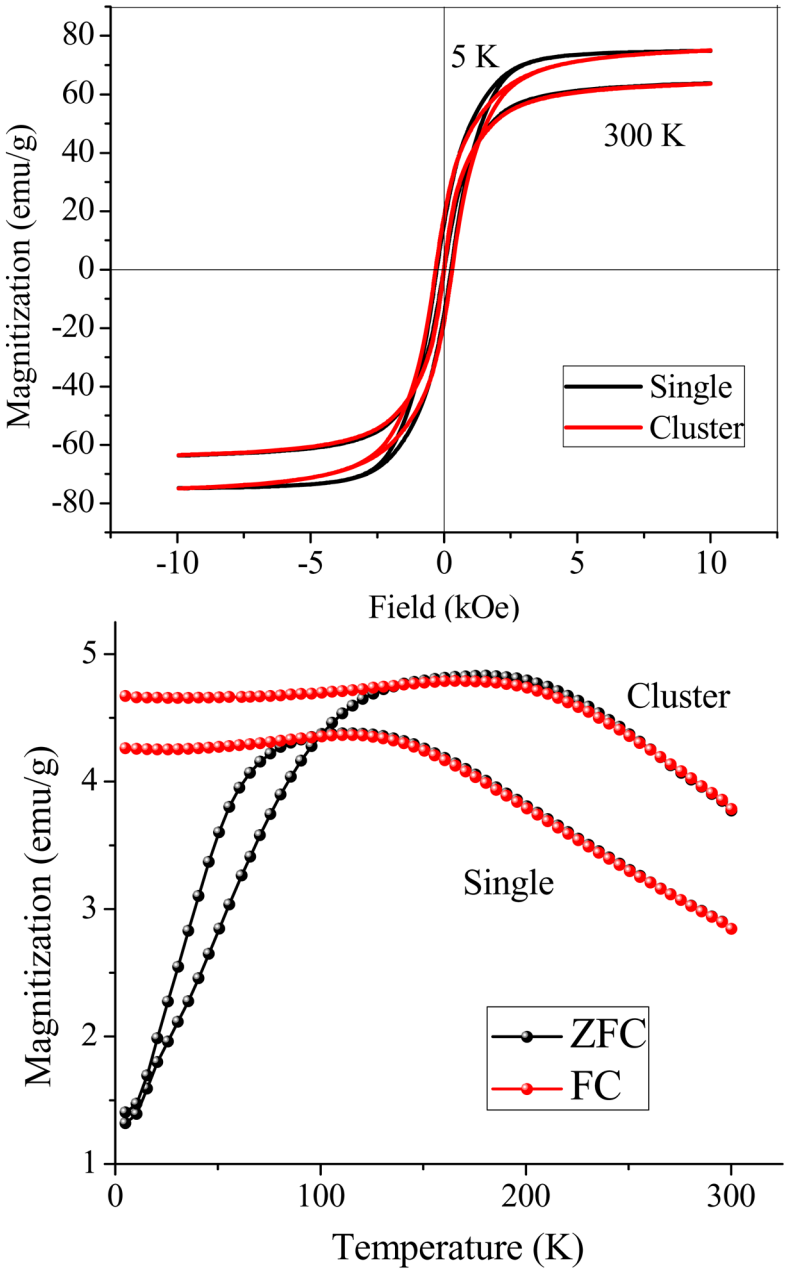

Figure 6.

Magnetization curves of NPCs and individual iron oxide NPs. Top: Mass magnetization as a function of field strength measured at 300 K and 5 K. At 300 K, both NPCs and individual NPs showed superparamagnetic behavior. Typical hysteresis loops were observed at 5 K, and NPCs exhibited coercivity very close to the individual NPs, probably because of the coexistence of anisotropic and random assembly of NPs during the cluster formation process; Bottom: ZFC/FC measured at 50 Oe, the blocking temperature had shifted from 111 K to 181 K after cluster formation, which indicates that strong dipole –dipole interactions had taken place among nanoparticles inside the clusters.

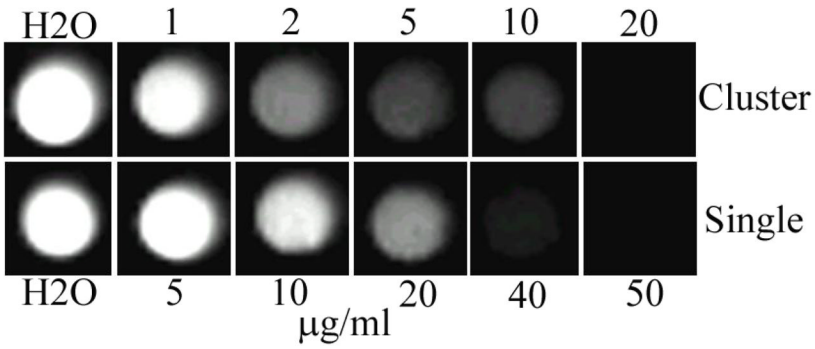

Figure 7.
MRI images of NPCs and individual NPs with different concentrations in water. The darker contrast shown at a lower concentration for NPCs indicates that in the clustered form, a lower concentration of Fe is needed to obtain a desired contrast.

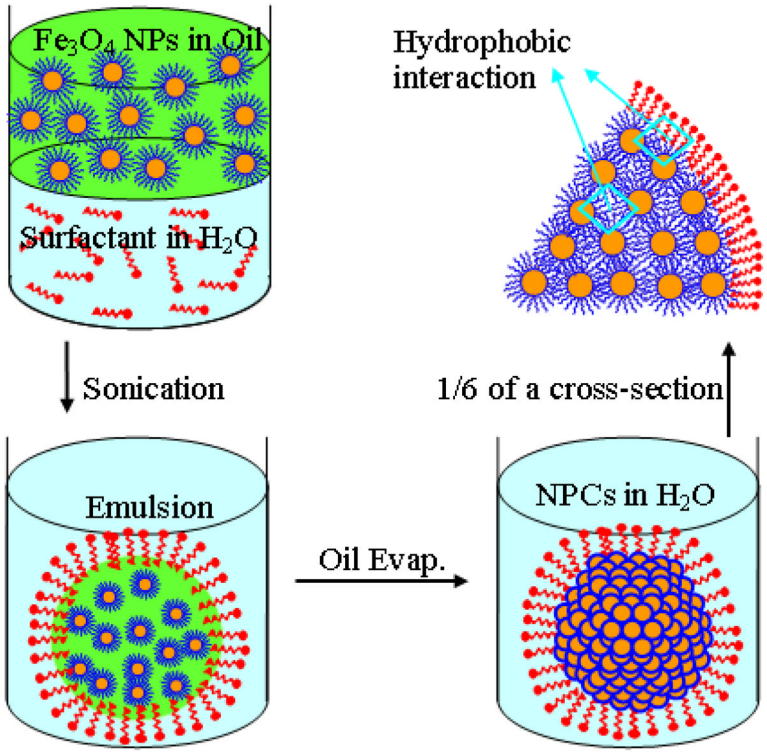

Scheme 1.
Schematic diagram of the formation of NPCs.

Table 1

Surface charge density and average diameter of NPCs using different stabilizers.*

Stabilizer	Zeta Potential (mV)	Ave. Dia. (nm)	
		First**	Secondary**
CTAB	+49	78	33
PEI	+33	88	42
PAA	−56	72	30
PSS	−64	65	28

* The NPCs were made from 3 nm hydrophobic iron oxide nanoparticles in hexane.

** First= first centrifuge run at 10,000 rpm for 5 min; Second= second run at 15,000 rpm for 20 min.